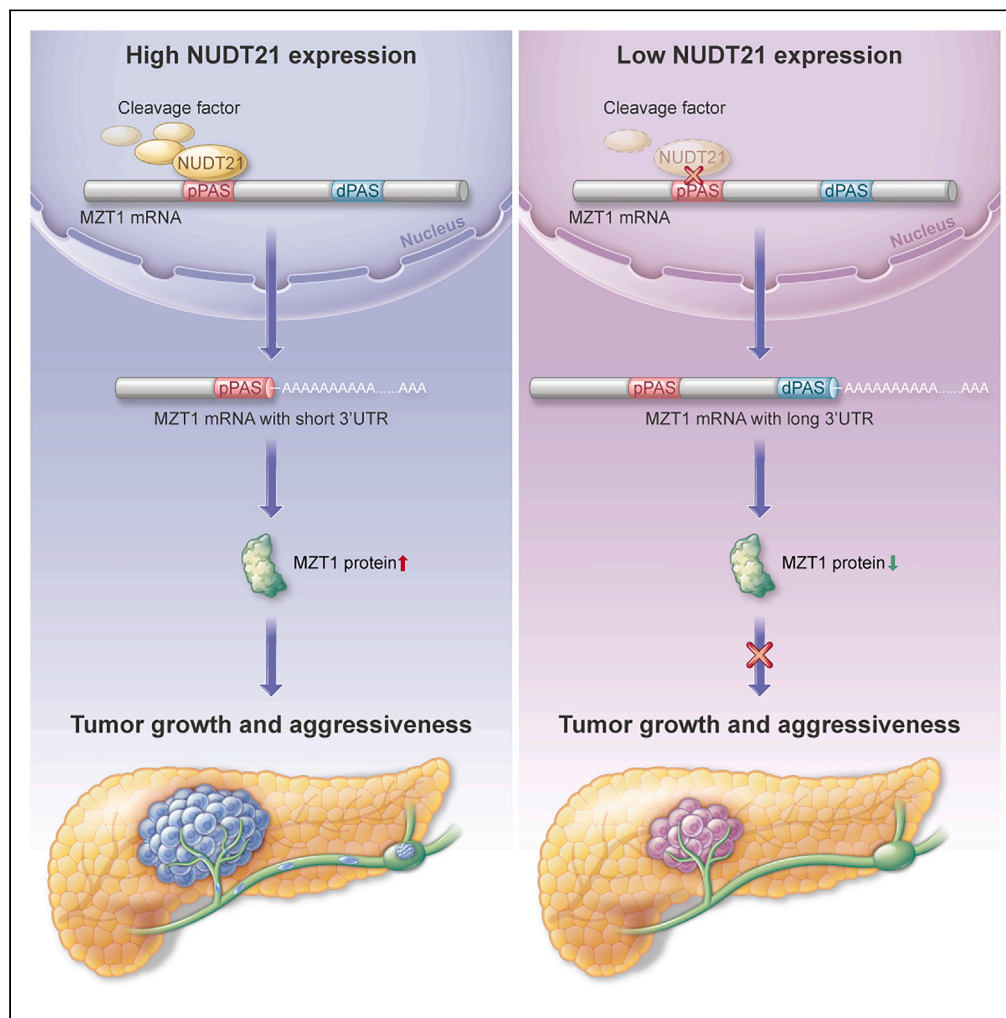**Article**

Nudt21-mediated alternative polyadenylation of MZT1 3'UTR contributes to pancreatic cancer progression

Yu Zhou, Jiabin Yang, Leyi Huang, Chao Liu, Min Yu, Rufu Chen, Quanbo Zhou

chenrufu@gdph.org.cn (R.C.)
zhouqbo@mail.sysu.edu.cn (Q.Z.)

Highlights

APA-mediated 3'UTR shortening events are increased in liver metastasis of PC

The short-3'UTR isoform of MZT1 exerts enhanced metastatic effect

NUDT21 controls the stability and translation of MZT1 in an APA-dependent way

Article

Nudt21-mediated alternative polyadenylation of MZT1 3′UTR contributes to pancreatic cancer progression

Yu Zhou,[1,6] Jiabin Yang,[1,2,6] Leyi Huang,[3,4,6] Chao Liu,[5] Min Yu,[1] Rufu Chen,[1,*] and Quanbo Zhou[1,3,4,7,*]

SUMMARY

Alternative polyadenylation (APA) is an important post-transcriptional regulatory mechanism and is involved in many diseases, but its function and mechanism in regulating pancreatic cancer (PC) pathogenesis remain unclear. In this study, we found that the 3′ UTR shortening of MZT1 was the most prominent APA event in PC liver metastases. The short-3′UTR isoform exerted a stronger effect in promoting cell proliferation and migration both *in vitro* and *in vivo*. NUDT21, a core cleavage factor involved in APA, promoted the usage of proximal polyadenylation sites (PASs) on MZT1 mRNA by binding to the UGUA element located upstream of the proximal PAS. High percentage of distal polyA site usage index of MZT1 was significantly associated with a better prognosis. These findings demonstrate a crucial mechanism that NUDT21-mediated APA of MZT1 could promote the progression of PC. Our findings provided a better understanding of the connection between PC progression and APA machinery.

INTRODUCTION

Pancreatic cancer (PC) is hallmarked by aggressive tumor behavior. Despite the substantial progress in treatment modalities, the 5-year survival rate of all-stage newly diagnosed PC remains only 12%.[1] Therefore, exploring the molecular mechanisms underlying PC progression is crucial to improve treatment strategies.

It is well-established that mRNA serves as an inevitable connecting link for genetic information passing from DNA to protein.[2] Gene expression in higher eukaryotes requires multistep RNA processing events to format mature mRNA from immature, newly synthesized precursor mRNA (pre-mRNA). Pre-mRNA maturation includes 3′-end cleavage and polyadenylation, resulting in generating the 3′end, which is critical for mRNA function and stability.[3] Both cleavage and polyadenylation occur at polyadenylation sites (PASs), and previous work has revealed that more than 70% of eukaryotic genes contain multiple alternative PASs.[4] Differential usage of PASs can lead to the formation of distinct mRNA isoforms with different 3′termini, a phenomenon termed alternative polyadenylation (APA) which is involved in various gene regulation steps including mRNA stability, translation, nuclear export, localization, and protein diversification.[5]

Extensive APA events occur during the pathophysiology of many diseases including cancers, and recent studies have highlighted the importance of APA dysregulation in both tumor initiation and progression.[6] In cancers, APA is believed to promote tumorigenesis and progression by increasing the expression of oncogenes and reducing the expression of tumor suppressor genes.[7] APA-mediated global shortening of 3′ UTRs has been identified in various cancers; these APA events represent potentially novel prognostic biomarkers and may uncover novel mechanisms for the regulation of cancer driver genes.[8] However, most APA events in cancers as well as their mechanisms remain poorly understood. On the other hand, a growing number of APA-regulatory factors have been identified and characterized in the past decade, mainly including four different protein subcomplexes: the cleavage and polyadenylation specificity factor (CPSF), cleavage stimulation factor (CstF), mammalian cleavage factor I (CFIm) and cleavage factor II (CFIIm).[5] Some proteins of the subunit of the aforementioned complexes have been proved to act as oncogenes or tumor suppressors.[9,10] Nudix hydrolase 21 (NUDT21), also termed CFIm25 (cleavage and polyadenylation-specific factor 5, 25-kD subunit), is one of the major factors that govern APA of the 3′ UTR.[11,12] NUDT21 functions by binding to the UGUA motifs upstream to the poly(A)-sites and then lead to alternative usage of PASs.[13] NUDT21 was found to be dysregulated in kinds of malignancies and to play indispensable roles on tumorigenesis, acting either as oncogenes or tumor suppressor genes.[14–16]

[1]Department of Pancreatic Surgery, Department of General Surgery, Guangdong Provincial People's Hospital (Guangdong Academy of Medical Sciences), Southern Medical University, Guangzhou, Guangdong Province, China
[2]School of Medicine, South China University of Technology, Guangzhou, Guangdong Province, China
[3]Department of Pancreatobiliary Surgery, Sun Yat-sen Memorial Hospital, Sun Yat-sen University, Guangzhou, Guangdong Province, China
[4]Guangdong Provincial Key Laboratory of Malignant Tumor Epigenetics and Gene Regulation Medical Research Center, Sun Yat-sen Memorial Hospital, Sun Yat-sen University, Guangzhou, Guangdong Province, China
[5]Department of Pathology, Guangdong Provincial People's Hospital, Guangdong Academy of Medical Sciences, Guangzhou, Guangdong Province, China
[6]These authors contributed equally
[7]Lead contact
*Correspondence: chenrufu@gdph.org.cn (R.C.), zhouqbo@mail.sysu.edu.cn (Q.Z.)
https://doi.org/10.1016/j.isci.2024.108822

Although previous studies have identified aberrant APA events in PC, and some diagnostic and therapeutic targets have been discovered by focusing on APA in PC,[17] the mechanisms of APA in the progression of PC, particularly in metastasis, remain largely unclear. In this study, we identified PC progression-associated APA events by comparing metastatic lesions with primary lesions. We discovered abnormal alterations in the 3′ UTR length of MZT1 specifically in metastatic lesions. We demonstrated that NUDT21 promoted the progression of PC by promoting the production of long 3′UTR MZT1 (mitotic spindle organizing protein 1) isoform, which was correlated with increased stability and translational efficacy of MZT1 mRNA. This present study further expands our understanding of the crucial role of APA in PC, emphasizing the significance of NUDT21-mediated 3′ UTR shortening of MZT1 in the progression of PC.

RESULTS

High-throughput 3′UTR sequencing revealed the 3′UTR of MZT1 was significantly shortened in liver metastatic lesions of pancreatic cancer

To identify the 3′UTR alterations in liver metastases derived from PC, we performed IVT-SAPAS (*in vitro* transcription-sequencing APA sites) to profile the APA sites of three matched pairs of primary tumors and matched liver metastases. We calculated the average 3′UTR length of each sample by weighting and normalizing the length of the tandem 3′UTR. The average 3′UTR length of genes in liver metastatic lesions was slightly increased than that of primary PC tumors (Figure 1A). To identify the genes with significantly altered 3′UTR length, we performed the test of linear trend as previously described.[18] In each pair of PC tissues, we found a significantly changed length of 3′UTR in dozens of genes (Figures 1B–1D). We also found the global 3′UTR alternations did not correlate with the transcriptional difference, suggesting the way of APA exerts its biological function in PC metastasis is not primarily through regulating mRNA expression transcriptionally, and the effect of APA on mRNA expression may focus on some specific targets. We next compared the APA events in the three pairs of primary cancer and metastases and found that the MZT1 predominantly displayed shortened 3′UTR length in metastatic lesions, and it was the only gene with pCor index over 0.2 in all three groups (Figures 1E–1H).

As shown in Figure 1I, IVT-SAPAS showed the MZT1 had two main APA isoform types, and two typical core APA elements, the AAUAAA and UGUA,[5] were observed upstream of the proximal PAS. Meanwhile, a CA sequence which is often immediately 5′ to the cleavage site[5] was identified just following the proximal PAS, supporting a potential stronger APA modification effect at the proximal PAS of MZT1. Therefore, to further confirm the presence of different usage of the PASs of MZT1, the 3′UTR sequences of MZT1 were verified by 3′ RACE and Sanger sequencing. As shown in the Figures 1J and 1K, the exact site of proximal PAS and distal PAS was confirmed.

Next, the increased usage of proximal PAS of MZT1 in liver metastatic lesions was further determined in 10 primary-liver metastasis pairs by qRT-PCR by using specific primers targeting the MZT1 coding region or its distal 3′UTR. As shown in Figure 1L, the expression of the long-3′UTR isoform of MZT1 was significantly increased in the primary PC tissues, which supports the increased usage of proximal PAS in MZT1 3′UTR. Moreover, MZT1 protein expression was obviously higher in liver metastasis than in the corresponding primary PC (Figure 1M).

Short 3′UTR isoform of MZT1 exerts enhanced metastatic effect than the long 3′UTR isoform both *in vitro* and *in vivo*

The aforementioned results revealed that the short isoform of MZT1 is associated with liver metastasis in PC. Therefore, the next question was whether the isoform selection and the metastasis and progression of PC are functionally linked. Bioinformatics analysis indicated a significant correlation between high MZT1 expression and enrichment of pathways related to tumor metastasis and cell adhesion in the TCGA-PAAD dataset (Figures S1 and S2). Next, we stably transfected short- or long-3′UTR isoforms of MZT1 into PANC-1 and MIA Paca-2 cell lines, two PC cell lines had moderate and low MZT1 expression, respectively (Figures 2A and 2B). We found that enhanced expression of the short-3′UTR MTZ1 isoform dramatically promoted the proliferation and migration ability of both cell lines (Figures 2C–2E). Further *in vivo* experiments also confirmed that increased expression of short-3′UTR isoform in PC cells substantially enhanced the abilities of subcutaneous tumor formation when compared with that of overexpressed long-3′UTR isoform (Figures 2F–2H). Meanwhile, *in vivo* mice metastasis models were used to evaluate the roles of two MZT1 isoforms in regulating PC metastasis (Figures 2I and 2J). Differences in the numbers and maximum diameters of liver/lung metastases for mice in each group were observed under the microscope (Figure 2K). We found that overexpression of short-3′UTR isoform dramatically promoted the metastasis ability of PC cells. The number of both liver and lung metastatic nodules in the short-isoform overexpressing group was significantly increased than that of the control group or of the MZT1 long-isoform overexpressing group (Figures 2K and 2L). In addition, the maximum diameter of liver metastasis and lung metastasis in each mouse were evaluated (Figures 2K and 2M), and we found the diameters of the metastases in both lung and liver were significantly increased in the group with overexpression of short MZT1 isoform. Collectively, these results showed that the short-isoform of MZT1 was able to promote PC cell proliferation and metastasis better than the long-isoform both *in vitro* and *in vivo*.

3′ UTR shortening increased MZT1 protein level through enhancing stability and translation efficiency of its mRNA

Since the MZT1 short-3′UTR isoform exerts enhanced oncogenic capacity, and we observed that increased expression of the short-3′UTR MZT1 isoform substantially upregulated its protein level, we further evaluated how the APA affects MZT1 expression. Quantification of the mRNA levels of MZT1 was performed by qRT-PCR. Compared with the long-3′UTR isoform, short-3′UTR had a more significant positive impact on expression of mRNA (Figure 3A) and protein (Figure 3B) in both PANC-1 and MIA Paca-2 cell lines. Therefore, we next evaluated the effect of APA on the translational efficiency of MZT1 mRNA by performing polysome profiling. The cellular lysate was prepared, and then the highly translated mRNAs and poorly translated mRNAs were separated by ultracentrifugation in a sucrose density gradient (Figure 3C). The
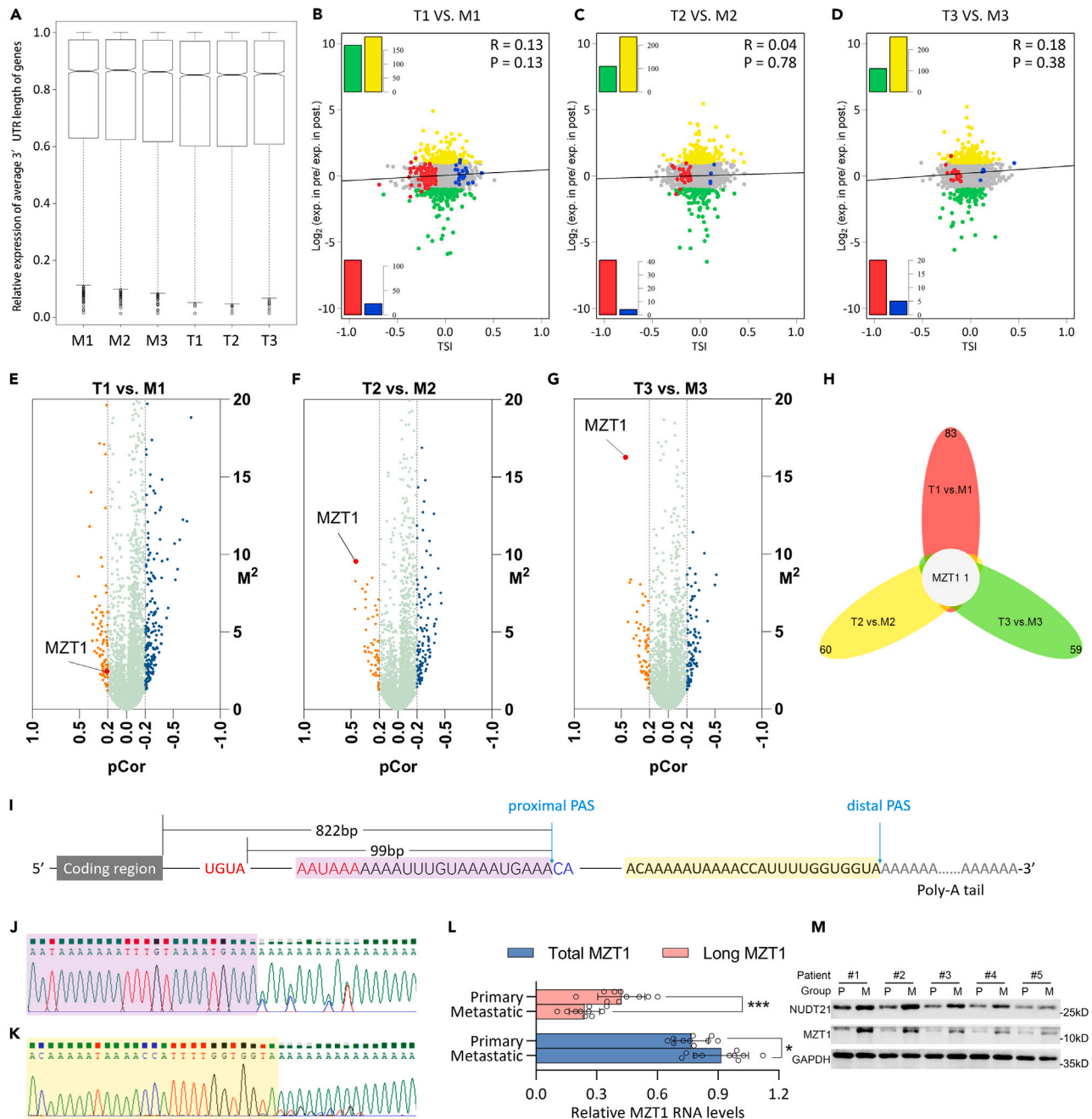
Figure 1. High-throughput 3'UTR sequencing revealed the 3'UTR of MZT1 was significantly shortened in liver metastatic lesions of pancreatic cancer

(A) Boxplot of standardized 3'UTR length of genes with tandem APA sites in each sample.

(B–D) APA site switching and changes in gene expression levels for each paired primary tumor and liver metastasis. The x axis denotes TSI. A positive TSI value indicates that longer tandem 3'UTRs was observed in primary tumor and vice versa. The y axis denotes the logarithm of the expression level of genes, and a positive value indicates the expression was upregulated in the primary tumor and vice versa.

(E–G) Volcano plots showing the results of linear trend test for 3'UTR length differences between pair of the primary tumor and liver metastasis for each gene.

(H) Venn diagram showing the overlap of poly(A) site-switched genes with pCor >0.2.

(I) Schematic diagram illustrating the PAS sites of MZT1 according to IVT-SAPAS result.

(J and K) Results of Sanger sequencing show the proximal PAS (J) and distal PAS (K).

(L) MZT1 transcripts with 3' UTRs of different lengths were identified by qRT-PCR in 10 paired primary and metastatic tumors. The levels of long transcripts and total transcripts are shown.

(M) The protein expression of NUDT21 and MZT1 in the 5 paired primary and metastatic tumors was evaluated by western blot. Data were presented as the mean ± SD of independent experiments. *p < 0.05, ***p < 0.001.
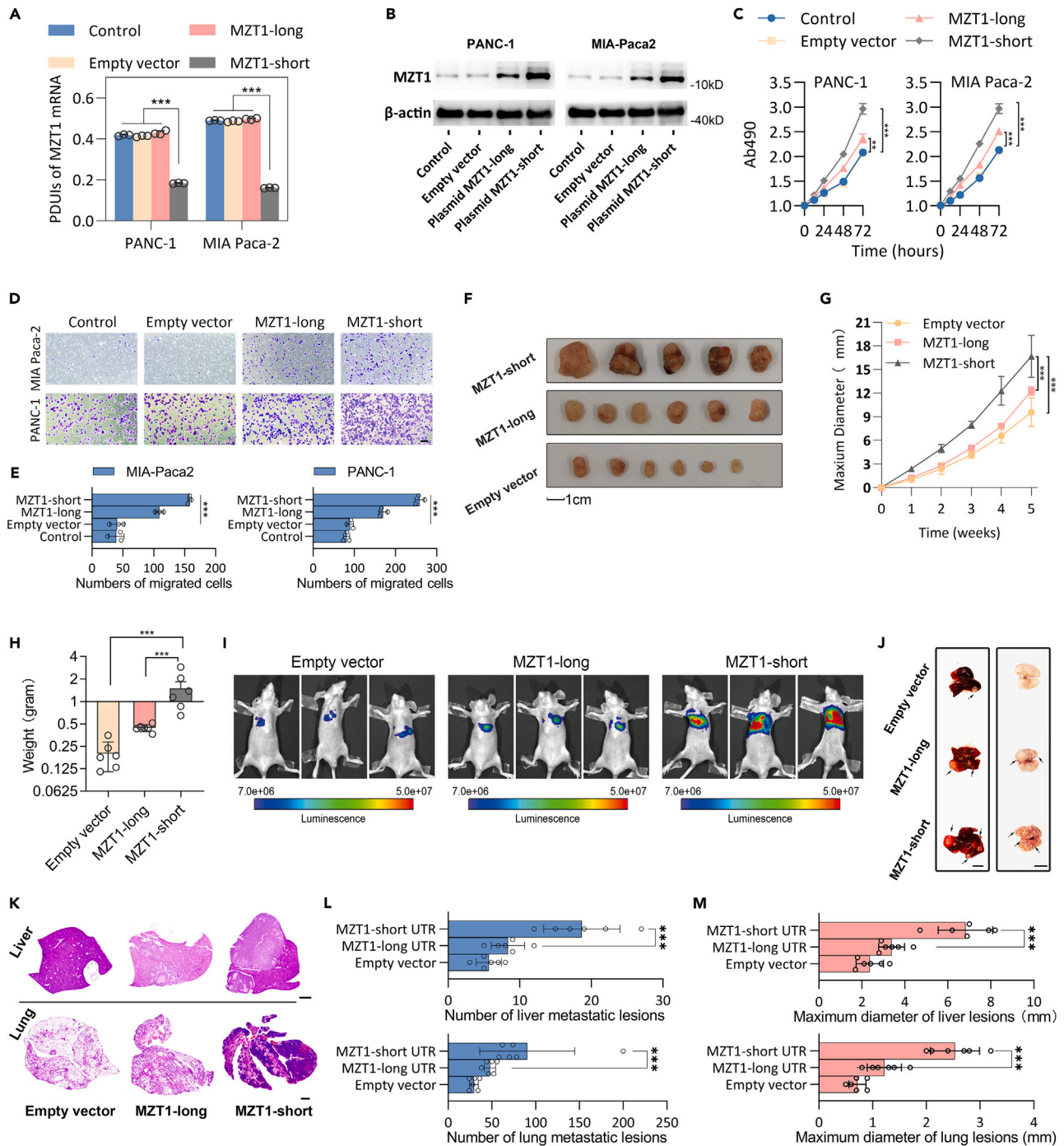
Figure 2. Short 3′UTR isoform of MZT1 exerts an enhanced tumor-promoting effect

(A and B) qRT-PCR (A) and western blot (B) results show the fold change in percentage of distal polyA site usage index (PDUI) of MZT1 and in MZT1 protein expression in PC cell lines transfected with the MZT1 short- or long-3′UTR isoform.

(C) Growth curves for PANC-1 and Mia Paca-2 cells stably transfected with empty vector, vector to overexpress MZT1 short-3′UTR isoform, or vector to overexpress MZT1 long-3′UTR isoform.

(D and E) Transwell assay analyses of the invasion ability of the indicated PC cell lines. Scale bar: 100 μm.

(F) Images of the xenograft tumors formed in nude mice injected with PANC-1 cells transfected with empty vector, MZT1 short- and long-3′UTR isoforms. Scale bar: 1 cm.

(G) Growth curves of xenograft tumors in mice.

(H) Weights of xenograft tumors.

Figure 2. Continued

(I) The effect of MZT1 isoforms on metastasis ability was evaluated by the *in vivo* metastasis model. Representative bioluminescent images in the indicated group are shown.

(J) Representative images of the liver (left panel) and lung (right panel) metastatic nodules (black arrows) are shown. Scale bar: 1 cm.

(K) Sections of the liver and lung from the mice were analyzed by HE staining. Scale bar: 2000 μm.

(L) The numbers of metastasis nodules from each mouse were counted. The numbers of metastasis nodules in the liver or lung were counted through histological examination of 10 sections from each organ.

(M) The maximum diameter of metastasis nodules from each mouse was measured. Data were presented as the mean ± SD of independent experiments. **$p < 0.01$, ***$p < 0.001$.

subsequent qRT-PCR analysis revealed that MZT1 mRNA in translation-active fractions (>80S) contained a significantly higher proportion of short-3′UTR isoform than those in non-translating (<40 S) and translation initiation (40S, 60S, 80S monosomes, and <80S) fractions (Figure 3D), indicating the translation efficiency of the short-3′UTR isoform of MZT1 was significantly higher than that of the long-3′UTR isoform. Translational efficiencies of MZT1 3′UTR were additionally measured through luciferase activity (Figure 3E). As expected, the luciferase reporters containing short-3′UTR region of MZT1 displayed significantly higher luciferase activities as compared to those containing the long-3′UTR of MZT1.

In addition, compared with the overexpression of the long-3′UTR isoform, we found overexpression of the short-3′UTR isoform led to a more pronounced upregulation of total MZT1 mRNA, we therefore analyzed the difference in RNA stability between the two isoforms by performing actinomycin D assay. The qRT-PCR analysis of the MZT1 isoforms at the different stages after actinomycin D treatment revealed that the degradation rate of the long-3′UTR MZT1 isoform was faster than that of the short-3′UTR isoform (Figures 3F and 3G), suggesting that the MZT1 mRNA with short-3′UTR was more stable than those with long-3′UTR. At last, the correlation between MZT1 protein and its isoforms was examined in human PC tissues from 68 cases. As shown in Figure 3H, immunohistochemistry for MZT1 was performed on PC samples, and we found that samples with higher MZT1 protein expression usually showed significantly decreased PDUIs of MZT1 mRNA and significantly increased total MZT1 mRNA (Figures 3I and 3J), which supported the aforementioned findings that short-3′UTR isoform was correlated with both higher translation efficiency and more RNA stability.

NUDT21 promotes the usage of the proximal PAS of MZT1

We next investigated which polyadenylation factor was responsible for the enhanced production of the short MZT1 isoform. Different siRNAs targeting well-known polyadenylation factors were transfected separately into HeLa cells to identify the factor whose expression best correlates with the production of the short 3′UTR isoform of MZT1. Among all factors examined, we found that silencing of NUDT21 was most closely associated with a decreased level of short 3′UTR isoform and increased PDUI value of MZT1 (Figures 4A and 4B). To further investigate the effect of NUDT21 on the protein expression and usage of the PAS of MZT1, we selected two cell lines, Capan-2 and PANC-1, with respectively high and moderate NUDT21 protein expression (Figure 4C), to construct cell lines with stable knockdown of NUDT21 (Figures 4D and S3). We observed an obvious reduction in the MZT1 protein expression following NUDT21 knockdown in both cell lines (Figure 4E). Additionally, the PDUIs of MZT1 were significantly increased in both cell lines after downregulating NUDT21 (Figure 4F). Meanwhile, the mRNA level of MZT1 was also downregulated after the NUDT21 knockdown (Figure 4G). The aforementioned *in vitro* results were further supported by the evidence from the public database, including the TCGA (The Cancer Genome Atlas), CCLE (Cancer Cell Line Encyclopedia), and TC3A (The Cancer 3′ UTR Atlas) database. As shown in Figures 4H–4J, we found that the NUDT21 expression was significantly and positively correlated with MZT1 expression in both cell lines (Figure 4H) and human tissues (Figure 4I), and the NUDT21 expression was negatively related to MZT1 PDUI (Figure 4J). The aforementioned experiments suggest that NUDT21 might play a major role in regulating the alternative usage of PAS of MZT1.

NUDT21 regulates the stability and translational efficiency of MZT1 and binds to it in a UGUA element-dependent manner

We next sought to confirm the regulatory effect of NUDT21 on the mRNA stability and translational efficiency of MZT1. In PANC-1 and Capan-2 cells, knockdown of NUDT21 significantly accelerated degradation of the MZT1 mRNA (Figures 5A and 5B), in which the short-3′UTR isoform of MZT1 was significantly much more stable than the long-3′UTR isoform (Figure 5C). To examine the effect of NUDT21 on the efficiency of MZT1 translation, we performed ribosome profiling and found that NUDT21 knockdown significantly decreased MZT1 mRNA loading onto translating polyribosomes (Figures 5D–5F). Next, we used the protein synthesis inhibitor CHX and the proteasome inhibitor MG132 to further study the regulatory mechanism of NUDT21 on MZT1 expression. The results showed that CHX, but not MG132, abolished NUDT21 knockdown-induced downregulation of MZT1 protein expression in PANC-1 cells (Figure 5G), suggesting that NUDT21 regulates MZT1 protein expression by modulating the translation of MZT1 mRNA as opposed to protein degradation.

To further confirm the binding between NUDT21 and *MZT1*, RNA immunoprecipitation (RIP) assays were performed. Through RIP assay, we determined that NUDT21 interacts with *MZT1* (Figure 5H). As cleavage and polyadenylation are suggested to be controlled by *cis* elements located upstream and downstream of the PAS, and the upstream element UGUA is the well-known specific bingeing sequence of NUDT21, we then wondered if the APA regulation of MZT1 3′UTR is directly controlled by NUDT21 through being recruited to its classical binding site. We mutated the UGUA motif that locates upstream of the proximal PAS of MZT1 (Figure 5I), and the RNA electrophoretic mobility shift assay (RNA EMSA) further displayed that NUDT21 binds to MZT1, and the binding between NUDT21 and MZT1 was diminished in UGUA-mutated MZT1 (Figure 5J). These results suggested that NUDT21 directly binds to MZT1 mainly via the upstream UGUA element.
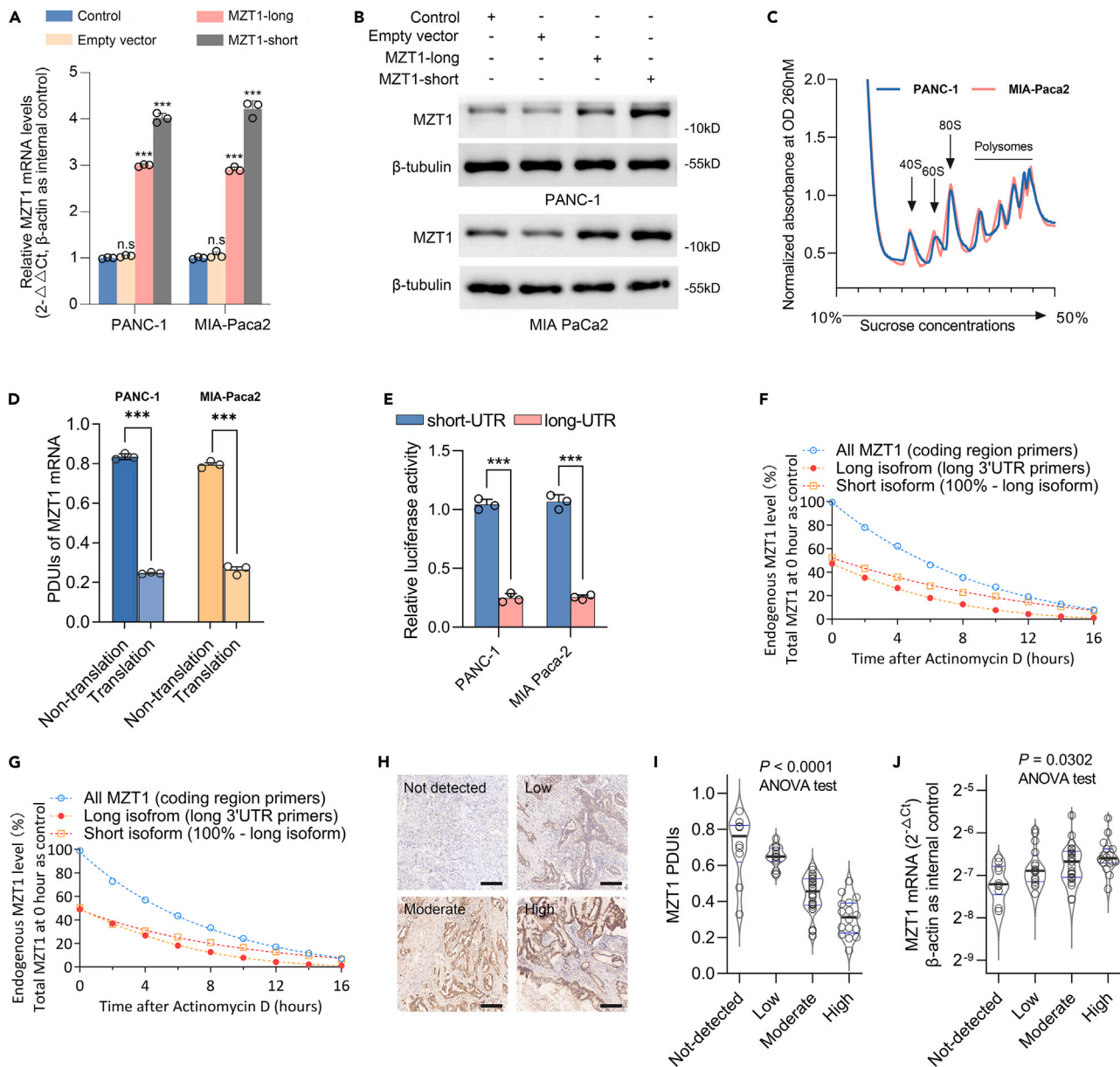
Figure 3. 3′ UTR shortening increased stability and translation efficiency of MZT1 mRNA

(A) Bar graphs showing the mRNA levels quantified by qRT-PCR in PANC-1 and Mia Paca-2 cells.

(B) Western blot analysis showing the protein expression levels of MZT1 in different treatment groups of PANC-1 and Mia Paca-2 cells.

(C) Polysome profiling of PANC-1 and Mia Paca-2 cells was performed.

(D) Comparison of PDUIs of MZT1 mRNA in non-ribosome portion and in polysome portion.

(E) The long- or short-3′UTR fragments were cloned into the luciferase reporter vector. The effect of 3′UTRs on translation activity in PANC-1 and Mia Paca-2 cells was examined by luciferase assay.

(F and G) RNA stability assays were performed in PANC-1 and Mia Paca-2 cells using Actinomycin D to disrupt RNA synthesis.

(H) Representative immunohistochemical (IHC) images of pancreatic cancer tissues with the differential expression levels of MZT1. Scale bar: 200 μm.

(I and J) The correlation between MZT1 PDUI (I)/MZT1 mRNA expression (J) and MZT1 IHC staining level was examined by one-way ANOVA test. Data were presented as the mean $\pm$ SD of independent experiments. ***p < 0.001.

Short-3′UTR isoform of MZT1 mediates the cancer-promoting role of NUDT21

To further investigate the associations between MZT1 polyadenylation and NUDT21, we further evaluated whether the different APA isoforms of MZT1 play different roles as a downstream factor of NUDT21. Based on the aforementioned result (Figure 4C), we chose two cell lines, Capan-2 and BXPC-3, with high NUDT21 expression levels to establish stable NUDT21 knockdown cell lines for this investigation (Figure S3).
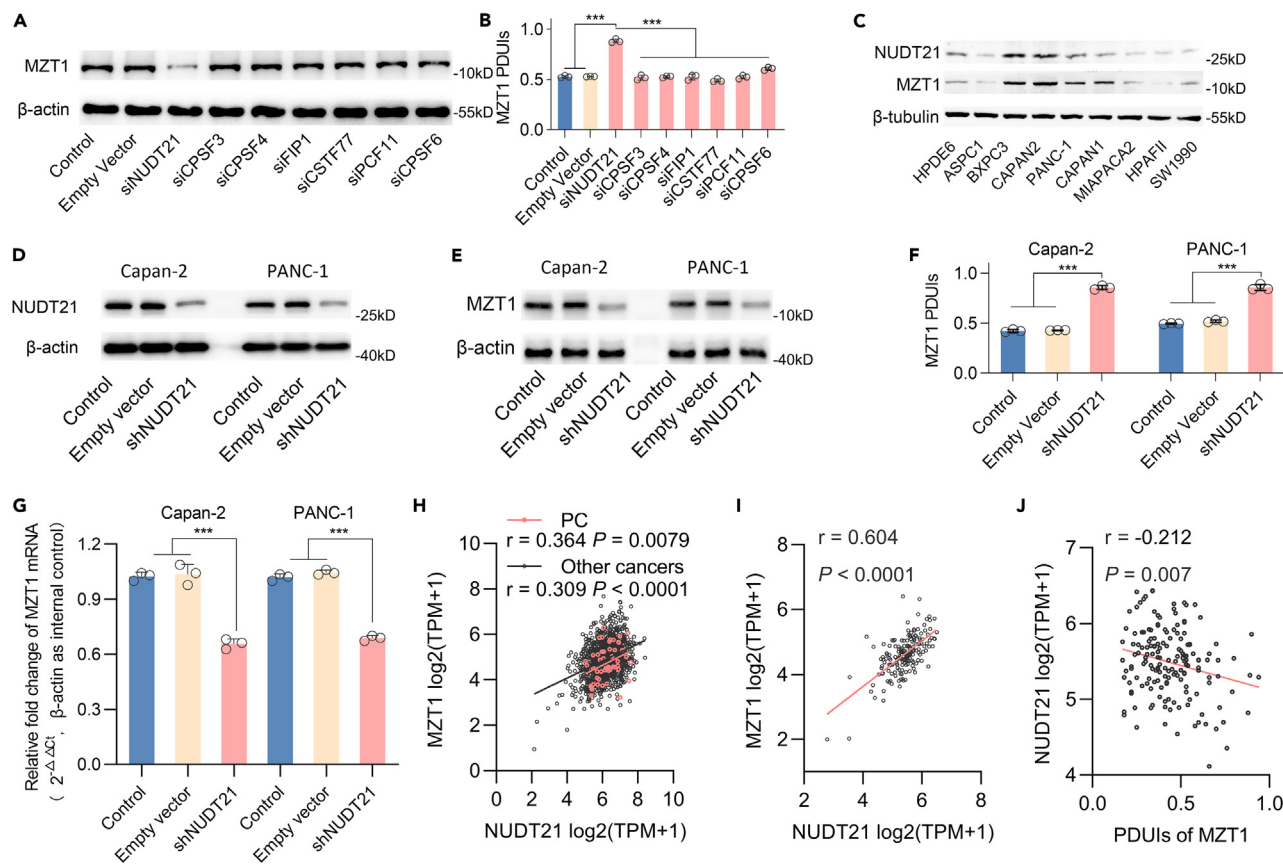
Figure 4. NUDT21 correlates with the usage of the proximal PAS of MZT1

(A) Western blot results show the protein levels of MZT1 upon siRNA silencing of each indicated APA factors in PANC-1 cells.

(B) qRT-PCR results of MZT1 PDUI in PANC-1 cells after silencing of each APA factor as indicated.

(C) Western blot analysis of NUDT21 and MZT1 protein expression in various common pancreatic cancer cell lines.

(D) Stable knockdown of NUDT21 in Capan-2 cell line and PANC-1 cell line.

(E) The effect of stable knockdown of NUDT21 on MZT1 protein expression was analyzed by western blot.

(F and G) The effect of stable knockdown of NUDT21 on MZT1 PDUI (F) and MZT1 mRNA level (G) was analyzed by qRT-PCR.

(H) The correlation between NUDT21 expression and MZT1 mRNA level in cancer cell lines was examined by correlation analysis based on CCLE data. Red dots indicate pancreatic cancer cell lines.

(I) The correlation between NUDT21 expression and MZT1 mRNA level in pancreatic cancer was examined based on TCGA data.

(J) The correlation between NUDT21 expression and MZT1 PDUI in pancreatic cancer was examined based on the combination of TCGA and TC3A datasets. Data were presented as the mean $\pm$ SD of independent experiments. ***$p < 0.001$.

In vitro, cell proliferation assays and colony formation analyses both showed that NUDT21 knockdown remarkably reduced cell proliferation and clonogenic capacity of PC cells (Figures 6A–6C). Transwell assay further showed that after knockdown of NUDT21, the numbers of migrated cells were significantly reduced when compared to that of the control cells (Figures 6D and 6E). *In vivo*, Capan-2 cells with indicated treatments were inoculated into nude mice by subcutaneous injection. As expected, the group of mice injected with Capan-2 cells underwent NUDT21 knockdown developed remarkably smaller and others (Figures 6F–6H). Meanwhile, overexpression of short isoform of MZT1, but not the long isoform, reversed the growth inhibition effect of NUDT21 knockdown (Figures 6F–6H). The protein level, mRNA level, and PDUIs of MZT1 were shown in Figures 6I–6K, respectively. In the following *in vivo* metastasis experiments, we observed that knockdown of NUDT1 significantly impaired the metastatic capacity of PC cells, which was also reversed following overexpression of the short isoform of MZT1 (Figures 6L–6N).

MZT1-PDUI^high^/NUDT21^low^ is defined as a PC subpopulation with long survival

The prognostic value of MZT1 PDUIs and MZT1 mRNA levels in PC patients were confirmed through the combined use of TC3A data and TCGA data. A total of 178 patients were included in the study on the mRNA expression levels of MZT1 and NUDT21 and their prognostic significance. Among them, 160 patients were included in the study on the association between MZT1 PDUI and prognosis after excluding patients with incomputable PDUI values (Table S1). Patients with shorter MZT1 3′UTR displayed significantly poor survival, while MZT1
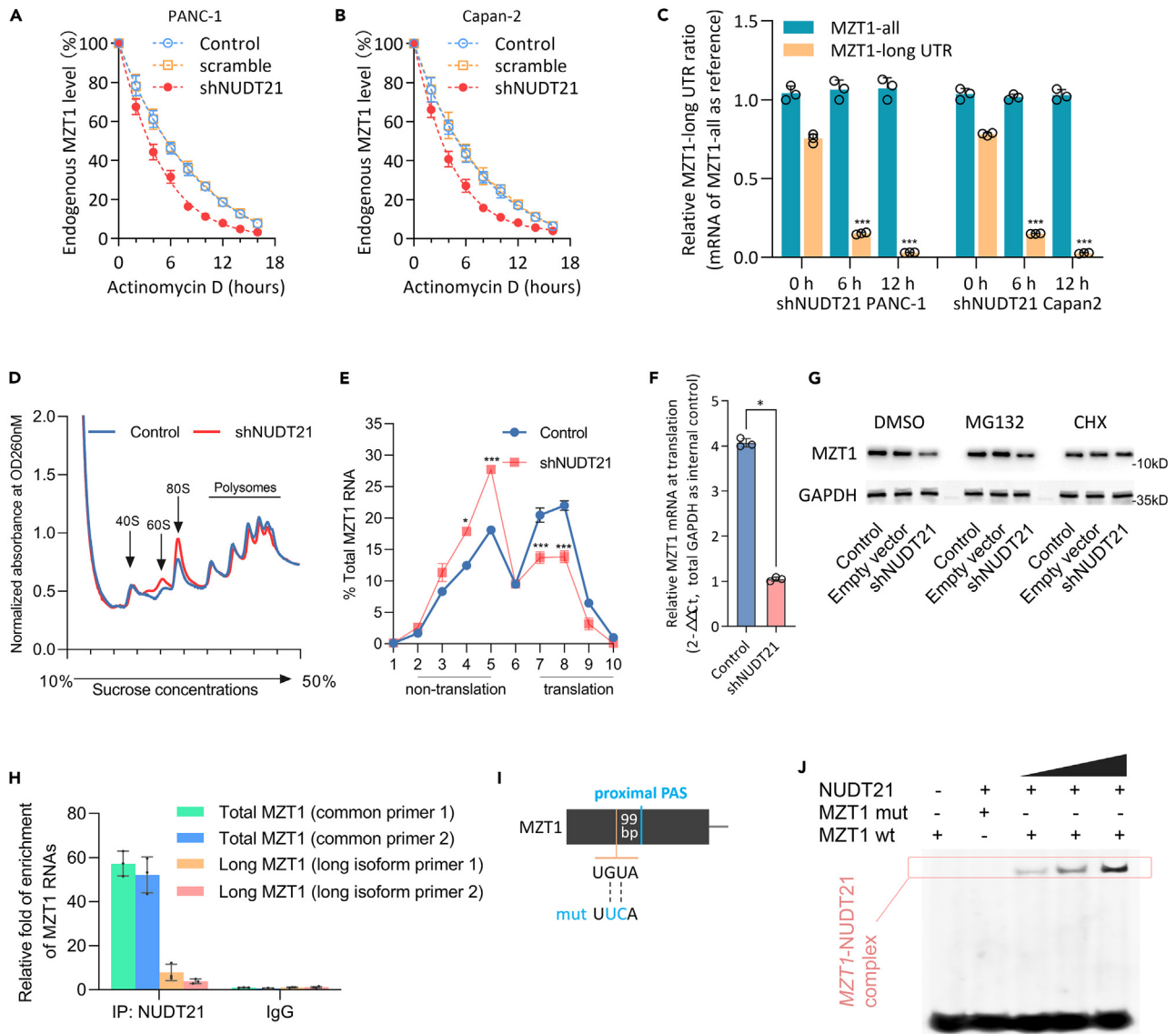
Figure 5. NUDT21 regulates the stability and translational efficiency of MZT1 and binds to MZT1 in a UGUA element-dependent manner

(A and B) Actinomycin D assays show the effect of NUDT21 knockdown on the stability of MZT1 mRNA in PANC-1 (A) and Capan-2 (B) cells.

(C) Differences in the proportion of MZT1 isoforms during the indicated time point during the actinomycin D assay were examined by qRT-PCR.

(D) Polysome profiling of Capan-2 cells with stable transfection of empty vector or NUDT21 shRNA.

(E and F) Analysis of MZT1 mRNA in non-translating portion vs. in translating portion.

(G) The effect of NUDT21 knockdown on MZT1 protein expression was examined under the treatment of MG132 or CHX.

(H) RIP assays show the association between NUDT21 and MZT1 mRNA.

(I and J) Biotin-labelled MZT1 oligonucleotides containing wild-type UGUA motif or mutant motif (I) were incubated with NUDT21 protein and then subjected to EMSA assay (J). Data were presented as the mean $\pm$ SD of independent experiments. $*p < 0.05$, $***p < 0.001$.

mRNA expression had no significant association with the prognosis (Figures 7A–7F). Additionally, multivariate Cox regression analyses were performed to confirm whether MZT1 was an independent risk factor for overall survival and progression-free survival of patients with PC after adjusting the main prognostic clinical factors. As shown in Figure 7G, increased PDUI of MZT1 was an independent determinant of lower risk for both death (HR = 0.207, 95%CI 0.052–0.815, p = 0.024) and tumor recurrence (HR = 0.177, 95%CI 0.048–0.647, p = 0.009). We further divided the PC patients into four groups based on the MZT1 PDUI (PDUI > 0.5, high vs. ≤0.5, low) and NUDT21 expression (top 50%, high vs. bottom 50%, low). As shown in Figure 7H, in TCGA data, the group with MZT1-PDUI^high/NUDT21^low exhibited a significantly improved prognosis compared to the other 3 subgroups. The 5-year OS and 5-year PFS were 67.1% and 52.5% in the group of MZT1-PDUI^high/NUDT21-^low. No more death was seen after 2 years in the patients of the MZT1-PDUI^high/NUDT21^low group. Furthermore, the prognostic significance of
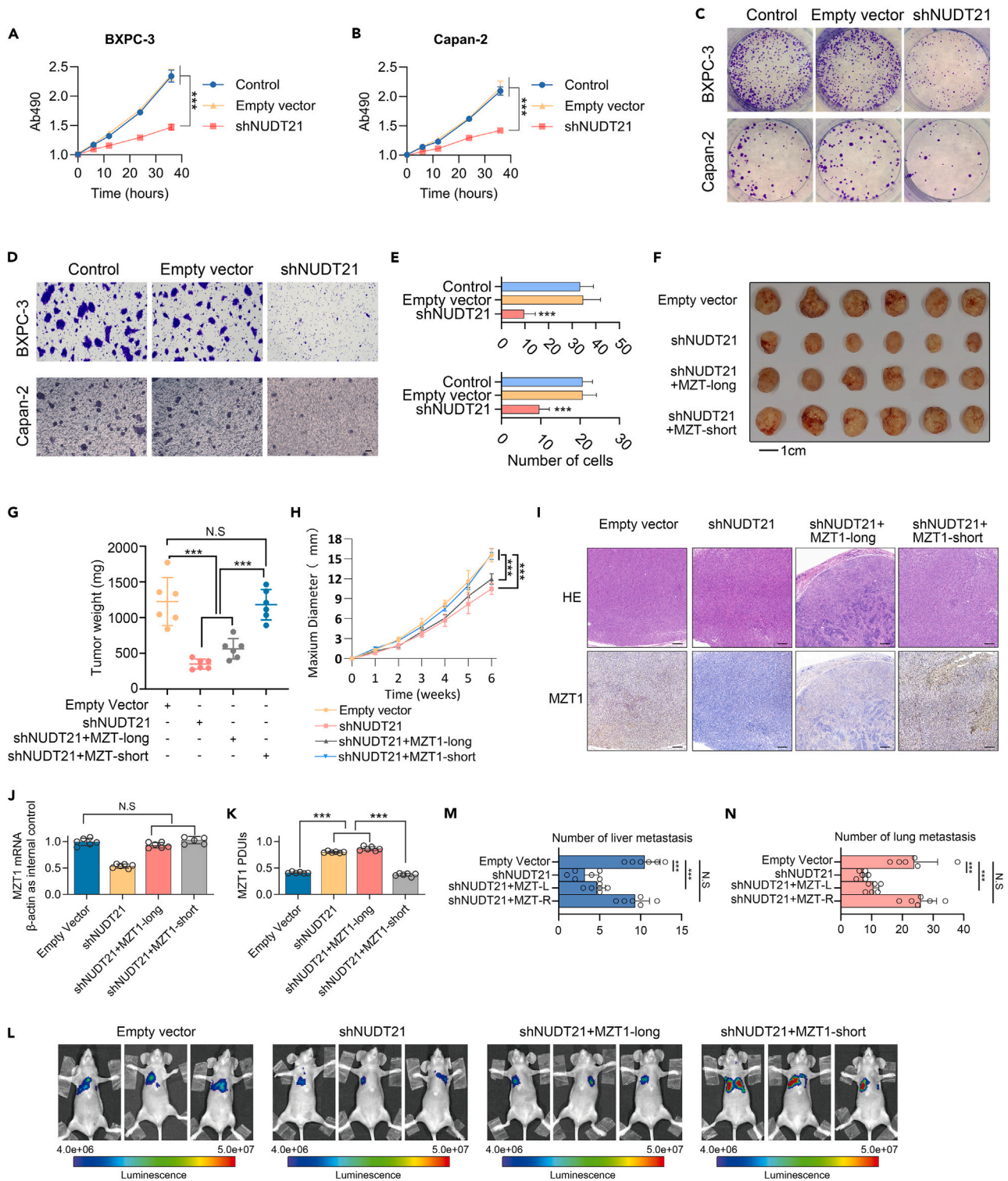
Figure 6. Overexpression of short isoform of MZT1 reversed the tumor suppressive effect of NUDT21 knockdown

Cell proliferation assays (A and B) and colony formation assays (C) showing the growth of pancreatic cells treated with NUDT21 knockdown.

(D and E) Transwell assays in pancreatic cancer cell lines treated with NUDT21 knockdown, statistics are shown with bar graph in (E). Scale bar: 100 μm.

(F) Representative pictures of the xenograft tumors formed in nude mice injected with Capan-2 cells with indicated treatments after six weeks. Scale bar: 1 cm.

(G and H) The tumor weight of xenograft tumors (G) and tumor diameters (H) in nude mice are shown.

Figure 6. Continued

(I) IHC assays showing the MZT1 protein level in xenograft tumors. Scale bar: 100 μm.

(J and K) Bar charts showing the level of MZT1 mRNA (J) and MZT1 PDUIs (K) in xenograft tumors.

(L) Representative *in vivo* imaging pictures of the mouse metastasis model.

(M) The number of liver metastasis and lung metastasis (N) were quantitatively analyzed. Data were presented as the mean ± SD of independent experiments. ***$p < 0.001$.

the aforementioned subgroups was validated in our center (Figure 7H, the GDPH cohort data panels), which also demonstrating that the MZT1-PDUIhigh/NUDT21low subgroup exhibited a significantly improved prognosis compared to the other three subgroups.

DISCUSSION

A comprehensive understanding of the molecular mechanisms underlying the aggressive behaviors of PC might help in identifying useful prognostic indicators and therapeutic targets for this dismal disease. Human cancer is a complex disease driven by the activation of oncogenes and/or inactivation of tumor suppressors. With the recent rapid advances in sequencing technologies, genome-wide profiling of APA sites has been performed in a variety of species, tissues, and disease states,[19–21] and numerous evidence has revealed that APA is an important regulatory mechanism for the activation of oncogenes.[10,22,23] Recent studies have provided confirmation that dysregulation of a wide range of APA events is involved in PC. The pan-cancer analysis conducted by Chan et al. revealed the widespread occurrence of 3′ UTR splicing events in cancer and found evidence of 3′ UTR shortening in PC.[24] Venkat et al. focused on PC and suggested that APA is an underappreciated driver of pro-tumorigenic gene expression in this dismal disease.[17] However, the specific role and mechanisms of APA in PC, especially regarding the alterations in APA in metastatic lesions, are still far from being fully elucidated.

In the current study, by using 3T-seq, we identified the 3′UTR shorting of MZT1 as an important APA event in PC progression. Based on further *in vitro* and *in vivo* experiments, bioinformatics, and clinical data analysis, we unearth a novel mechanism by which NUDT21 promotes the progression of PC via promoting the alternative usage of proximal PAS of MZT1 mRNA, which leads to increased stability and translational efficiency of MZT1 mRNA and higher MZT1 protein level. Our study has unveiled a novel APA event associated with the progression of PC: the shortening of the 3′ UTR of MZT1 mRNA. Moreover, this APA event regulates the expression of MZT1 protein through both mRNA stability and translation efficiency. These findings expand our understanding of APA events related to the progression of PC.

For the first time, we have uncovered that the shortening of the 3′ UTR of MZT1 mRNA is an APA event associated with the progression of PC. In humans, MZT1 plays an essential role in mitotic spindle formation as a component of the γ-tubulin ring complex,[25] which is a crucial component of the centrosome responsible for nucleation of microtubules and plays important role in cellular homeostasis and cell survival. The centrosome, the main microtubule-organizing center of human cells, coordinates cell migration, cell polarity, signal transduction pathways, and chromosome segregation in mitosis.[26] It was shown that centrosome amplification is sufficient to induce tumor formation.[27–29] Studies have confirmed that MZT1 is key for centrosome formation and duplication.[30,31] MZT1 is also essentially important for maintaining and regulating the eukaryotic cytoskeleton, nuclear shaping and nuclear envelope,[32–34] all of which are critically involved in the onset and development of tumorigenesis.[35,36] Therefore, although the role of MZT1 in cancers has so far not been studied, it was not surprising our findings uncovered a pro-oncogenic role for MZT1 in PC. The role of MZT1 in malignancies warrants further investigation.

This study discovered that NUDT21 is a key regulator of the length of the 3′ UTR of MZT1. NUDT21 also known as CFIm25 is the key subunit of the core polyadenylation complex cleavage factor I (CFI).[12] Previous works suggested that downregulation of subunits of the CFI would result in increased use of upstream PASs,[37,38] which seemed to support the tumor suppressor role of NUDT21 since the hypothesis suggests the majority of APA events have shorter 3′UTRs in cancers.[8,23] However, the role of NUDT21 in tumors remains controversial.[39] Zheng et al. firstly revealed that NUDT21 knockdown inhibits proliferation and promotes apoptosis of PC cells, which supporting the cancer-promoting role of NUDT21 in PC; however, they did not elucidate the specific mechanism of NUDT21 in PC from the perspective of APA.[40] Surprisingly, we found the 3′UTR length of MZT1 was significantly increased upon NUDT21 knockdown, suggesting an unconventional role of NUDT21 in favoring the proximal PASs of these genes. Then an important question that emerged was, which gene or genes was the main target of NUDT21 in PC. By using RIP assay, we found the NUDT21 protein mainly interacted with MZT1 mRNA. It has been well established that CFIm25 is both necessary and sufficient for sequence-specific binding of the poly(A) site upstream element UGUA.[13] The CFI complex exists as a dimer, and the CFIm25 homodimer binds two UGUA elements (usually separated by a sequence of variable length) upstream to a PAS and therapy allowed facilitates the selection of the PAS.[41] Our analysis of the MZT1 nucleotide sequence upstream of proximal PAS revealed the existence of typical UGUA elements. Importantly, the other APA elements, including AAUAAA, U-rich and GU-rich elements,[5] were also identified close to the proximal PAS of MZT1 mRNA. In PC cells, we confirmed that downregulation of NUDT21 diminished the percentage of MZT1 isoform with short 3′UTR. A negative correlation between NUDT21 expression and percentage usage of the distal PAS of MZT1 in PC was confirmed by both data from clinical specimens and a public cohort with a large sample size. Moreover, *in vitro* mutation of the UGUA element near the proximal PAS attenuated the interaction of NUDT21 on MZT1. All the aforementioned findings together provide evidence for NUDT21 in directly regulating the APA of MZT1 by promoting the usage of its proximal PAS.

Using the transcription inhibitor actinomycin D to measure mRNA stability, the long isoform of MZT1 was found to be less stable than the short isoform. Besides, previous studies have reported a role for 3′ UTR length in regulating translation,[42] and our study also demonstrated that the short isoform of MZT1 was correlated with enhanced translational efficiency. In our experiments with MG132 or CHX, we confirmed that NUDT21 regulates MZT1 by influencing its translation but not degradation. Therefore, the altered 3′UTR length of MZT1 may contribute
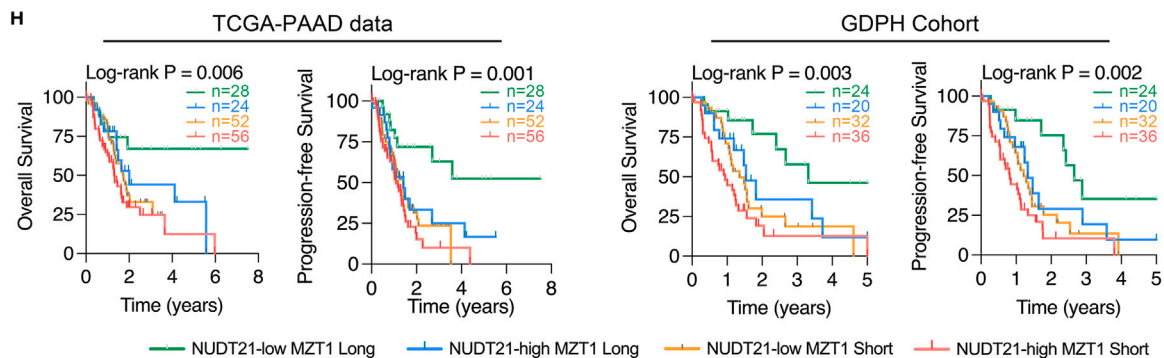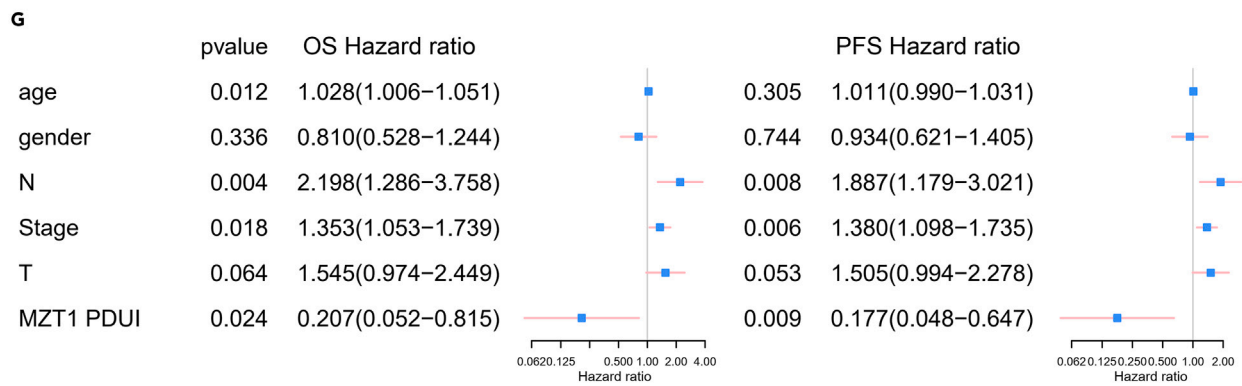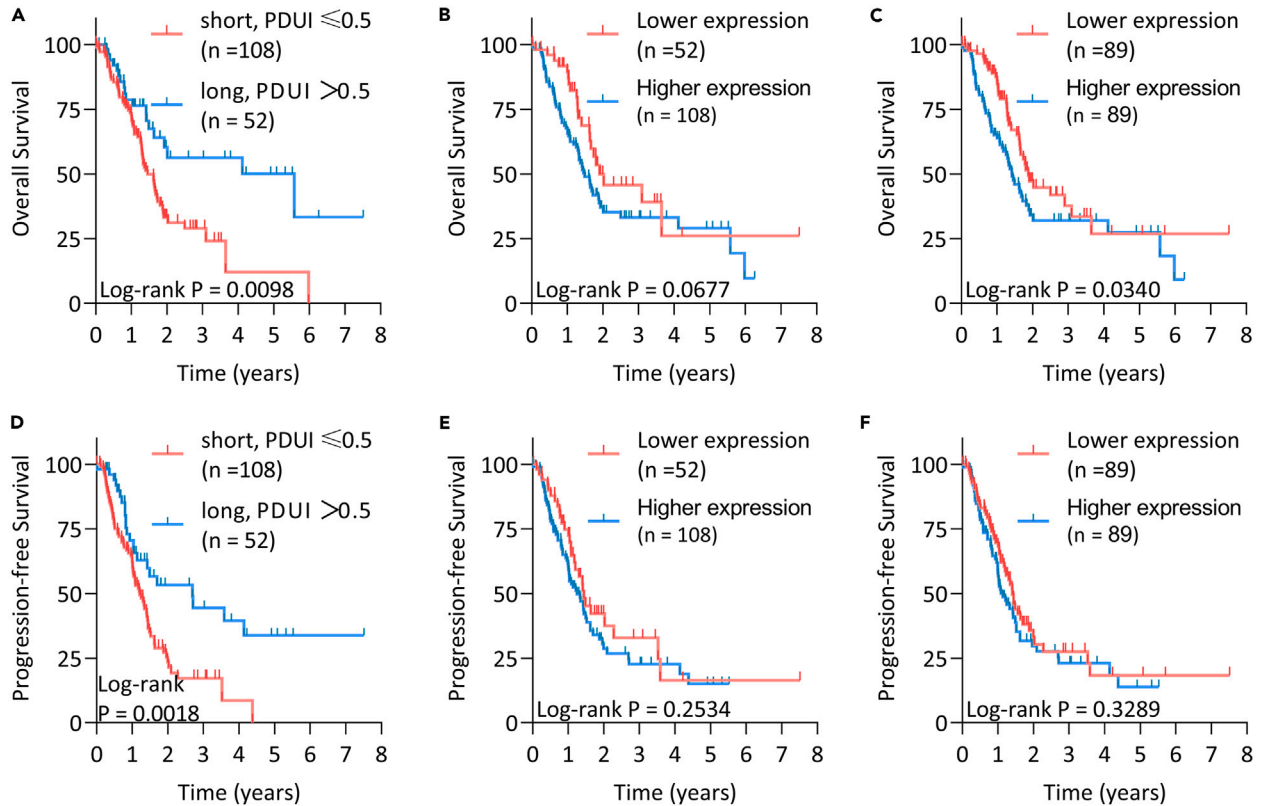
A

Overall Survival

short, PDUI ⩽0.5 (n =108)
long, PDUI >0.5 (n = 52)

Log-rank P = 0.0098

Time (years)

B

Overall Survival

Lower expression (n =52)
Higher expression (n = 108)

Log-rank P = 0.0677

Time (years)

C

Overall Survival

Lower expression (n =89)
Higher expression (n = 89)

Log-rank P = 0.0340

Time (years)

D

Progression-free Survival

short, PDUI ⩽0.5 (n =108)
long, PDUI >0.5 (n = 52)

Log-rank P = 0.0018

Time (years)

E

Progression-free Survival

Lower expression (n =52)
Higher expression (n = 108)

Log-rank P = 0.2534

Time (years)

F

Progression-free Survival

Lower expression (n =89)
Higher expression (n = 89)

Log-rank P = 0.3289

Time (years)

G

	pvalue	OS Hazard ratio		pvalue	PFS Hazard ratio
age	0.012	1.028(1.006−1.051)		0.305	1.011(0.990−1.031)
gender	0.336	0.810(0.528−1.244)		0.744	0.934(0.621−1.405)
N	0.004	2.198(1.286−3.758)		0.008	1.887(1.179−3.021)
Stage	0.018	1.353(1.053−1.739)		0.006	1.380(1.098−1.735)
T	0.064	1.545(0.974−2.449)		0.053	1.505(0.994−2.278)
MZT1 PDUI	0.024	0.207(0.052−0.815)		0.009	0.177(0.048−0.647)

Hazard ratio
0.062 0.125 0.500 1.00 2.00 4.00

Hazard ratio
0.062 0.125 0.250 0.500 1.00 2.00

H

TCGA-PAAD data

Log-rank P = 0.006
Overall Survival
n=28
n=24
n=52
n=56
Time (years)

Log-rank P = 0.001
Progression-free Survival
n=28
n=24
n=52
n=56
Time (years)

GDPH Cohort

Log-rank P = 0.003
Overall Survival
n=24
n=20
n=32
n=36
Time (years)

Log-rank P = 0.002
Progression-free Survival
n=24
n=20
n=32
n=36
Time (years)

NUDT21-low MZT1 Long   NUDT21-high MZT1 Long   NUDT21-low MZT1 Short   NUDT21-high MZT1 Short

Figure 7. The prognostic value of MZT1 PDUI in pancreatic cancer

(A–C) Kaplan-Meier analysis with log rank test for overall survival (OS) of pancreatic cancer patients based on the data from the combination of TCGA and TC3A datasets, grouped according to MZT1 PDUIs (A) or MZT1 expression (B and C).

(D–F) Kaplan-Meier analysis with log rank test for progression-free survival (PFS) of pancreatic cancer patients based on the data from the combination of TCGA and TC3A datasets, grouped according to MZT1 PDUIs (D) or MZT1 expression (E and F).

(G) Independent risk factors of OS and PFS for pancreatic cancer patients in multivariate logistic regression analysis.

(H) Kaplan-Meier OS curves and Kaplan-Meier PFS curves for pancreatic cancer patients are based on the data from two datasets, the combination of TCGA-PAAD data, and the GDPH cohort. Patients were categorized into four groups according to the MZT1 PDUI value (> 0.5, high vs. ≤0.5, low) and NUDT21 mRNA level (top 50%, high vs. bottom 50%, low).

to changing protein levels in a much more effective way than MZT1 mRNA itself. In line with this, the PDUIs of MZT1, which represent the changes in the 3′UTR length of this gene, were much more significantly correlated with the prognosis of PC patients in comparison with the levels of whole MZT1 mRNA. Collectively, we revealed a new efficient mechanism for regulating the MZT1 protein expression, which was hard to be revealed through traditional sequencing technology.

Our results unveil the oncogenic role of MZT1 in PC progression as well as the importance of the NUDT21/MZT1 APA axis in the regulation of MZT1 protein production in PC cells, which prompted us to further explore their prognostic value of them. The findings that MZT1 PDUI but not MZT1 mRNA level was significantly correlated with the prognosis of PC patients supported our aforementioned laboratory results that the post-transcriptional mechanism of MZT1 was much more important than the MZT1 mRNA level itself. In addition, it is worth noting that none of the MZT1 PDUI^{high}/NUDT21^{low} patients in the TCGA PC cohort had a recurrence or died after the second year. The 5-year survival rate and the 5-year progression-free survival rate was 67.1% and 52.5%, respectively, which was quite a favorable prognosis for this dismal disease. And no more death in the MZT1 PDUI^{high}/NUDT21^{low} patients was found since the second year. These results appear to reflect the important value of MZT1 PDUI^{high}/NUDT21^{low} in helping to differentiate PC patients with good prognosis from those with poor prognosis.In conclusion, our study identifies MZT1 as the direct target of NDT21 in PC cells. NUDT21 controls the stability and translation of MZT1 in an APA-dependent manner and affects the final protein level. The finding is that NUDT21-dependent APA regulation on MZT1 provided a novel oncogenic mechanism in PC and may serve as a promising candidate for the treatment of PC. The MZT1 PDUI^{high}/NUDT21^{low} patients had a significantly better prognosis than others.

Limitations of the study

At present, this study still has some limitations. Originally, the role and mechanism of different subtypes of MZT1 regulated by NUDT21 in tumor microenvironment needs to be further explored. Additionally, the specific mechanism by which MZT1 drives PC metastasis remains unclear. Subsequently, we proposed MZT1can be used as an effective biomarker for treatment, but the further transformation value of MZT1 *in vivo* needs to be further verified.

STAR★METHODS

Detailed methods are provided in the online version of this paper and include the following:

- KEY RESOURCES TABLE
- RESOURCE AVAILABILITY
  - Lead contact
  - Materials availability
  - Data and code availability
- EXPERIMENTAL MODEL AND STUDY PARTICIPANT DETAILS
  - Clinical samples
  - Cell lines and cell culture
  - *In vivo* xenograft tumor model
  - Ethical approval
- METHOD DETAILS
  - High-throughput APA sequencing
  - Actinomycin D assay
  - RNA interference and transfection
  - 3′Rapid Amplification of cDNA Ends (3′-RACE)
  - Colony formation assay
  - Scratch-wound healing
  - Transwell assays
  - Polysome fractionation
  - RNA isolation and quantitative real-time PCR (qRT–PCR)
  - Calculation of PDUI (Percentage of distal PAS usage)
  - Luciferase reporter assay

○ RNA immunoprecipitation (RIP) assay
○ Western blot
○ CHX and MG132 assay
○ Functional enrichment
● QUANTIFICATION AND STATISTICAL ANALYSIS

AUTHOR CONTRIBUTIONS

Q.B.Z. conceptualized and supervised this study. Y.Z., J.B.Y., and L.Y.H. performed most experiments. M.Y. and R.F.C. prepared samples, collected clinical data, and carried out data analysis. C.L. provided pathology expertise. Y.Z. wrote the original draft, Q.B.Z., J.B.Y., and L.Y.H. were involved in analyses, discussion, and manuscript preparation. All authors reviewed the manuscript.

DECLARATION OF INTERESTS

The authors declare no competing interests.

REFERENCES

1. Siegel, R.L., Miller, K.D., Wagle, N.S., and Jemal, A. (2023). Cancer statistics, 2023. CA. Cancer J. Clin. 73, 17–48.

2. Crick, F. (1970). Central dogma of molecular biology. Nature 227, 561–563.

3. Dutertre, M., Sfaxi, R., and Vagner, S. (2021). Reciprocal Links between Pre-messenger RNA 3′-End Processing and Genome Stability. Trends Biochem. Sci. 46, 579–594.

4. Shi, Y., and Manley, J.L. (2015). The end of the message: multiple protein-RNA interactions define the mRNA polyadenylation site. Genes Dev. 29, 889–897.

5. Tian, B., and Manley, J.L. (2017). Alternative polyadenylation of mRNA precursors. Nat. Rev. Mol. Cell Biol. 18, 18–30.

6. Gruber, A.J., and Zavolan, M. (2019). Alternative cleavage and polyadenylation in health and disease. Nat. Rev. Genet. 20, 599–614.

7. Masamha, C.P., and Wagner, E.J. (2018). The contribution of alternative polyadenylation to the cancer phenotype. Carcinogenesis 39, 2–10.

8. Feng, X., Li, L., Wagner, E.J., and Li, W. (2018). TC3A: The Cancer 3′ UTR Atlas. Nucleic Acids Res. 46, D1027–D1030.

9. Chen, X., Zhang, J.X., Luo, J.H., Wu, S., Yuan, G.J., Ma, N.F., Feng, Y., Cai, M.Y., Chen, R.X., Lu, J., et al. (2018). CSTF2-Induced Shortening of the RAC1 3′UTR Promotes the Pathogenesis of Urothelial Carcinoma of the Bladder. Cancer Res. 78, 5848–5862.

10. Tan, S., Zhang, M., Shi, X., Ding, K., Zhao, Q., Guo, Q., Wang, H., Wu, Z., Kang, Y., Zhu, T., et al. (2021). CPSF6 links alternative polyadenylation to metabolism adaption in hepatocellular carcinoma progression. J. Exp. Clin. Cancer Res. 40, 85.

11. Gruber, A.R., Martin, G., Keller, W., and Zavolan, M. (2012). Cleavage factor Im is a key regulator of 3′ UTR length. RNA Biol. 9, 1405–1412.

12. Martin, G., Gruber, A.R., Keller, W., and Zavolan, M. (2012). Genome-wide analysis of pre-mRNA 3′ end processing reveals a decisive role of human cleavage factor I in the regulation of 3′ UTR length. Cell Rep. 1, 753–763.

13. Yang, Q., Gilmartin, G.M., and Doublié, S. (2010). Structural basis of UGUA recognition by the Nudix protein CFI(m)25 and implications for a regulatory role in mRNA 3′ processing. Proc. Natl. Acad. Sci. USA 107, 10062–10067.

14. Xiong, M., Chen, L., Zhou, L., Ding, Y., Kazobinka, G., Chen, Z., and Hou, T. (2019). NUDT21 inhibits bladder cancer progression through ANXA2 and LIMK2 by alternative polyadenylation. Theranostics 9, 7156–7167.

15. Masamha, C.P., Xia, Z., Yang, J., Albrecht, T.R., Li, M., Shyu, A.B., Li, W., and Wagner, E.J. (2014). CFIm25 links alternative polyadenylation to glioblastoma tumour suppression. Nature 510, 412–416.

16. Liu, K., Wang, B.J., Han, W., Chi, C.H., Gu, C., Wang, Y., Fu, X., Huang, W., Liu, Z., and Song, X. (2020). CFIm25-regulated lncRNA acv3UTR promotes gastric tumorigenesis via miR-590-5p/YAP1 axis. Oncogene 39, 3075–3088.

17. Venkat, S., Tisdale, A.A., Schwarz, J.R., Alahmari, A.A., Maurer, H.C., Olive, K.P., Eng, K.H., and Feigin, M.E. (2020). Alternative polyadenylation drives oncogenic gene expression in pancreatic ductal adenocarcinoma. Genome Res. 30, 347–360.

18. Fu, Y., Chen, L., Chen, C., Ge, Y., Kang, M., Song, Z., Li, J., Feng, Y., Huo, Z., He, G., et al. (2018). Crosstalk between alternative polyadenylation and miRNAs in the regulation of protein translational efficiency. Genome Res. 28, 1656–1663.

19. Derti, A., Garrett-Engele, P., Macisaac, K.D., Stevens, R.C., Sriram, S., Chen, R., Rohl, C.A., Johnson, J.M., and Babak, T. (2012). A quantitative atlas of polyadenylation in five mammals. Genome Res. 22, 1173–1183.

20. Chen, W., Jia, Q., Song, Y., Fu, H., Wei, G., and Ni, T. (2017). Alternative Polyadenylation: Methods, Findings, and Impacts. Dev. Reprod. Biol. 15, 287–300.

21. Hoque, M., Ji, Z., Zheng, D., Luo, W., Li, W., You, B., Park, J.Y., Yehia, G., and Tian, B. (2013). Analysis of alternative cleavage and polyadenylation by 3′ region extraction and deep sequencing. Nat. Methods 10, 133–139.

22. Xing, Y., Chen, L., Gu, H., Yang, C., Zhao, J., Chen, Z., Xiong, M., Kazobinka, G., Liu, Y., and Hou, T. (2021). Downregulation of NUDT21 contributes to cervical cancer progression through alternative polyadenylation. Oncogene 40, 2051–2064.

23. Park, H.J., Ji, P., Kim, S., Xia, Z., Rodriguez, B., Li, L., Su, J., Chen, K., Masamha, C.P., Baillat, D., et al. (2018). 3′ UTR shortening represses tumor-suppressor genes in trans by disrupting ceRNA crosstalk. Nat. Genet. 50, 783–789.

24. Chan, J.J., Zhang, B., Chew, X.H., Salhi, A., Kwok, Z.H., Lim, C.Y., Desi, N., Subramaniam, N., Siemens, A., Kinanti, T., et al. (2022). Pan-cancer pervasive upregulation of 3′ UTR

splicing drives tumourigenesis. Nat. Cell Biol. *24*, 928–939.

25. Dhani, D.K., Goult, B.T., George, G.M., Rogerson, D.T., Bitton, D.A., Miller, C.J., Schwabe, J.W.R., and Tanaka, K. (2013). Mzt1/Tam4, a fission yeast MOZART1 homologue, is an essential component of the γ-tubulin complex and directly interacts with GCP3(Alp6). Mol. Biol. Cell *24*, 3337–3349.

26. Nigg, E.A., and Holland, A.J. (2018). Once and only once: mechanisms of centriole duplication and their deregulation in disease. Nat. Rev. Mol. Cell Biol. *19*, 297–312.

27. Levine, M.S., Bakker, B., Boeckx, B., Moyett, J., Lu, J., Vitre, B., Spierings, D.C., Lansdorp, P.M., Cleveland, D.W., Lambrechts, D., et al. (2017). Centrosome Amplification Is Sufficient to Promote Spontaneous Tumorigenesis in Mammals. Dev. Cell *40*, 313–322.e5.

28. Fan, G., Sun, L., Shan, P., Zhang, X., Huan, J., Zhang, X., Li, D., Wang, T., Wei, T., Zhang, X., et al. (2015). Loss of KLF14 triggers centrosome amplification and tumorigenesis. Nat. Commun. *6*, 8450.

29. Li, X., Song, N., Liu, L., Liu, X., Ding, X., Song, X., Yang, S., Shan, L., Zhou, X., Su, D., et al. (2017). USP9X regulates centrosome duplication and promotes breast carcinogenesis. Nat. Commun. *8*, 14866.

30. Jiang, P., Zheng, S., and Lu, L. (2018). Mitotic-Spindle Organizing Protein MztA Mediates Septation Signaling by Suppressing the Regulatory Subunit of Protein Phosphatase 2A-ParA in Aspergillus nidulans. Front. Microbiol. *9*, 988.

31. Masuda, H., and Toda, T. (2016). Synergistic role of fission yeast Alp16GCP6 and Mzt1MOZART1 in γ-tubulin complex recruitment to mitotic spindle pole bodies and spindle assembly. Mol. Biol. Cell *27*, 1753–1763.

32. Batzenschlager, M., Herzog, E., Houlné, G., Schmit, A.C., and Chabouté, M.E. (2014). GIP/MZT1 proteins orchestrate nuclear shaping. Front. Plant Sci. *5*, 29.

33. Sanchez, A.D., and Feldman, J.L. (2017). Microtubule-organizing centers: from the centrosome to non-centrosomal sites. Curr. Opin. Cell Biol. *44*, 93–101.

34. Zupa, E., Liu, P., Würtz, M., Schiebel, E., and Pfeffer, S. (2021). The structure of the γ-TuRC: a 25-years-old molecular puzzle. Curr. Opin. Struct. Biol. *66*, 15–21.

35. Denais, C.M., Gilbert, R.M., Isermann, P., McGregor, A.L., te Lindert, M., Weigelin, B., Davidson, P.M., Friedl, P., Wolf, K., and Lammerding, J. (2016). Nuclear envelope rupture and repair during cancer cell migration. Science *352*, 353–358.

36. Fife, C.M., McCarroll, J.A., and Kavallaris, M. (2014). Movers and shakers: cell cytoskeleton in cancer metastasis. Br. J. Pharmacol. *171*, 5507–5523.

37. Gennarino, V.A., Alcott, C.E., Chen, C.A., Chaudhury, A., Gillentine, M.A., Rosenfeld, J.A., Parikh, S., Wheless, J.W., Roeder, E.R., Horovitz, D.D.G., et al. (2015). NUDT21-spanning CNVs lead to neuropsychiatric disease and altered MeCP2 abundance via alternative polyadenylation. Elife *4*, e10782.

38. Li, W., You, B., Hoque, M., Zheng, D., Luo, W., Ji, Z., Park, J.Y., Gunderson, S.I., Kalsotra, A., Manley, J.L., and Tian, B. (2015). Systematic profiling of poly(A)+ transcripts modulated by core 3' end processing and splicing factors reveals regulatory rules of alternative cleavage and polyadenylation. PLoS Genet. *11*, e1005166.

39. Jafari Najaf Abadi, M.H., Shafabakhsh, R., Asemi, Z., Mirzaei, H.R., Sahebnasagh, R., Mirzaei, H., and Hamblin, M.R. (2019). CFIm25 and alternative polyadenylation: Conflicting roles in cancer. Cancer Lett. *459*, 112–121.

40. Zheng, Y.S., Chen, M.L., Lei, W.D., Zhu, S.L., You, X.Q., and Liu, Y. (2020). NUDT21 knockdown inhibits proliferation and promotes apoptosis of pancreatic ductal adenocarcinoma through EIF2 signaling. Exp. Cell Res. *395*, 112182.

41. Yang, Q., Coseno, M., Gilmartin, G.M., and Doublié, S. (2011). Crystal structure of a human cleavage factor CFI(m)25/CFI(m)68/RNA complex provides an insight into poly(A) site recognition and RNA looping. Structure *19*, 368–377.

42. Floor, S.N., and Doudna, J.A. (2016). Tunable protein synthesis by transcript isoforms in human cells. Elife *5*, e10921.

43. Fu, Y., Ge, Y., Sun, Y., Liang, J., Wan, L., Wu, X., and Xu, A. (2015). IVT-SAPAS: Low-Input and Rapid Method for Sequencing Alternative Polyadenylation Sites. PLoS One *10*, e0145477.

STAR★METHODS

KEY RESOURCES TABLE

REAGENT or RESOURCE	SOURCE	IDENTIFIER
Antibodies		
anti-NUDT21	Abcam	Cat# ab183660; RRID:AB_2827670
anti-MZT1	Sigma-Aldrich	Cat# HPA066715, RRID:AB_2685709
anti-MZT1	Thermo	Cat# PA5-71155; RRID:AB_2689872
anti-β-actin	Abcam	Cat# ab8226; RRID:AB_306371
anti-rabbit IgG-HRP	Cell Signaling Technology	Cat# 7074; RRID:AB_2099233
anti-mouse IgG-HRP	Cell Signaling Technology	Cat# 7076; RRID:AB_330924
NUDT21 Polyclonal antibody	Proteintech	Cat# 10322-1-AP; RRID:AB_2251496
Bacterial and virus strains		
pCDH-CMV-MZT1-UTR-CDS-short-EF1-copGFP-T2A-Puro	IGE (Guangzhou, China)	N/A
pCDH-CMV-MZT1-UTR-CDS-long-EF1-copGFP-T2A-Puro	IGE (Guangzhou, China)	N/A
psiCHECK2	Promega	N/A
Chemicals, peptides, and recombinant proteins		
actinomycin D	Sigma	Cat# 114666
4% paraformaldehyde	Yongjin Biotech	N/A
Crystal Violet Staining Solution	Beyotime	Cat# C0121-100ml
Trizol reagent	Takara	Cat# 9109
cycloheximide	MCE	Cat# HY-12320
sucrose gradient buffer	Sigma	Cat# 718033-8IN
cycloheximide	Abcam	Cat# ab120093
MG132	Selleck	Cat# MG132 1211877-36-9
Dulbecco's modified Eagle's medium (DMEM)	Gibco	Cat#11965092
Roswell Park Memorial Institute (RPMI) 1640	Gibco	Cat#11875093
Critical commercial assays		
Lipofectamine 3000	Invitrogen	Cat#L3000-015
5'/3' RACE Kit, 2ndGeneration	Roche	Cat#No. 03 353 621 001
PrimeScript RT Reagent Kit	Takara	Cat#RR047A
TB Green Premix Ex TaqTM kit	Takara	Cat#RR820A
Dual-Luciferase® Reporter Assay	Promega	Cat#E1960
Magna RIP™ RNA-Binding Protein Immunoprecipitation Kit	Millipore	Cat#17-700
bicinchoninic acid Protein Assay Kit	Thermo	Cat#23227
polyvinylidene difluoride membrane	Millipore	Cat#P3313-10EA
CCK-8 kit	Beyotime	Cat#C0037
Deposited data		
APA sequencing data	This study	PRJNA842954 https://www.ncbi.nlm.nih.gov/sra/docs/
TCGA pancreatic cancer cohort	The Cancer Genome Atlas (TCGA)	https://portal.gdc.cancer.gov/
TC3A pancreatic cancer cohort	The Cancer 3' UTR Atlas	http://tc3a.org
RNA-seq gene expression data	Cancer Cell Line Encyclopedia (CCLE)	https://sites.broadinstitute.org/ccle/datasets

Continued

REAGENT or RESOURCE	SOURCE	IDENTIFIER
Experimental models: Cell lines		
PANC-1	ATCC	Cat#CRL-1469MET, RRID: CVCL_A4BT
Capan-2	ATCC	Cat#HTB-80 ™RRID:CVCL_0026
AsPC-1	ATCC	Cat#CRL-1682,RRID:CVCL_0152
MIA Paca-2	ATCC	Cat#CRM-CRL-1420 RRID:CVCL_0428
SW1990	ATCC	Cat#CRL-2172 RRID:CVCL_1723
BxPC-3	ATCC	Cat#CRL-1687 RRID:CVCL_0186
HPAF-II	ATCC	Cat#BxPC-3 RRID:CVCL_0313
Hela	ATCC	Cat# CCL-2 RRID:CVCL_0030
HEK-293T	ATCC	Cat# CRL-1573, RRID:CVCL_0045
Experimental models: Organisms/strains		
Female NOD-SCID mice(6-weeks-old)	Guangdong Medical Laboratory Animal center	N/A
Oligonucleotides		
Primers for quantitative PCR: listed in Table S2	This study	N/A
Primers for siRNA sequence: listed in Table S2	This study	N/A
Primers for shRNA sequence: listed in Table S2	This study	N/A
Primers for quantitative RACE: listed in Table S2	This study	N/A
Software and algorithms		
GraphPad Prism software version 9.0.0	GraphPad Software	https://www.graphpad.com
R version 4.2.1	R Foundation for Statistical	https://cran.r-project.org/

RESOURCE AVAILABILITY

Lead contact

Further information and requests for resources and reagents should be directed to and will be fulfilled by the lead contact, Quanbo Zhou (zhouqbo@mail.sysu.edu.cn).

Materials availability

Plasmids and animal models generated in this paper will be shared freely upon request to the lead contact.

Data and code availability

Data: High-throughput APA sequencing data have been deposited in The Sequence Read Archive (SRA) (https://www.ncbi.nlm.nih.gov/sra/docs/): PRJNA842954.

Code: This paper does not report original code.

Any additional information required to reanalyze the data reported in this paper is available from the lead contact upon request.

EXPERIMENTAL MODEL AND STUDY PARTICIPANT DETAILS

Clinical samples

For high-throughput sequencing and western blot analysis, 10 paired samples of primary PDAC tumor and liver metastases were obtained for 10 patients during needle biopsy or abdominal exploration. For qRT-PCR and survival analysis, 112 patients diagnosed with pancreatic adeno-carcinoma underwent curative resection at Guangdong Provincial People's Hospital between May 2018 and Aug 2021 were collected. For immunohistochemistry analysis, primary PDAC tissues from 68 pancreatic adenocarcinoma patients who received surgical resection or surgical biopsy at Guangdong Provincial People's Hospital between May 2018 and June 2020 were collected. Immunohistochemistry was performed on paraffin-embedded pathological slides, while qRT-PCR was conducted on tissues preserved in liquid nitrogen. The frozen tissues

were collected on the day of surgery and immediately stored in liquid nitrogen after obtaining the surgical resection specimens at $-80°C$ until use.

Cell lines and cell culture

Human pancreatic cancer cell lines (PANC-1, Capan-2, Capan-1, AsPC-1, MIA Paca-2, SW1990, BxPC-3, HPAF-II), Hela cells and HEK-293T cells were obtained from the ATCC (American Type Culture Collection, Rockville, MD, USA) and maintained under standard conditions in cell culture flasks according to manufacturer's instruction.

In vivo xenograft tumor model

For subcutaneous tumor formation model, 5×10^6 cells with indicated treatment were injected into the right inguinal area of NOD-SCID mice (female, 6–8 weeks of age, 18–20 g), purchased from Guangdong Medical Laboratory Animal Center. Maximum length and width were recorded for each tumor per week. Tumor volume was calculated according to the formula Volume = $0.52 \times$ (length $\times$ width^2). Mice were sacrificed 6 weeks after injection or when any one of the tumors reached an estimated volume of 2,000 mm^3. *In vivo* metastasis model was carried out through intravenously injection of 2×10^5 PC cells through tail vein into each 6-week-old NOD-SCID mice. Lungs and livers were harvested 5 weeks post injection and analyzed for metastatic colonization by histology.

Ethical approval

This study was approved by the Institutional Ethics Committees of Guangdong Provincial People's Hospital. [Approval number: KY2023-720-01].

METHOD DETAILS

High-throughput APA sequencing

APA sequencing was performed with the IVT-SAPAS (*in vitro* transcription-sequencing alternative polyadenylation sites) method as described previously.[43] Briefly, a total of 500 ng RNA was randomly fragmented. The first round of reverse transcription was performed to synthesis first cDNA strand using oligonucleotide primers containing T7 promoter sequence. The second strand was synthesized, followed by *in vitro* transcription. The RNA products were purified by beads and reverse transcribed with random primers. PCR was then performed to amplify the cDNA. The products of PCR with 200–500 bp were purified by AMPure XP Beads (Beckman Coulter). Sequencing data was obtained with an Agilent 2100 Bioanalyzer, and reads were mapped to the human hg19 reference genome, and internal priming was filtered. The 3'UTR switching for each gene between the control group and experimental group was detected by a test of linear trend alternative to independence, as previously described.[18] Pearson correlation test was performed to generate an r value for each gene as described in previous study, where r>0 was regarded as lengthened 3'UTR, and r<0 was regarded as shorted 3'UTR.

Actinomycin D assay

PDAC cells were seeded in a 6-well plate overnight and then treated with 2 mg/L actinomycin D (Sigma, USA) at indicated time. qRT-PCR assay assessed the stability of MZT1 and its isoforms after cancer cells were harvested.

RNA interference and transfection

For overexpression of MZT1 isoforms, the ORF of human MZT1 together with either the short or long 3'UTR were synthesized by IGE (Guangzhou, China) and cloned into the lentiviral vector pCDH-CMV-MCS-EF1-CopGFP-T2A-puro at EcoRI and BamHI sites. Stable knockdown of NUDT21 was conducted through construct shRNA plasmid. Knockdown efficiency of two shRNAs targeting NUDT21 were evaluated, and the shRNA #1 was selected for further study (Figure S3). siRNA was used for transient gene knockdown studies. The siRNAs for NUDT21, FIP1, CPSF3, CPSF4, CSTF1, CstF77, CstF64, PCF11, and CPSF6 were designed. siRNAs transfection were performed with Lipofectamine 3000 (Invitrogen, CA, USA) according to the manufacturers' instructions. The details of RNA interference were shown in Table S2.

3'Rapid Amplification of cDNA Ends (3'-RACE)

For the detection of the APA status of MZT1 mRNA, 3'-RACE was performed. The sequences of the primers are listed in Table S2. The synthesized cDNA was used as a template for PCR, and the product was then purified after agarose gel electrophoresis. TA cloning was carried out by using the recovered gel as template followed by Sanger sequencing.

Colony formation assay

Fiver hundreds PDAC cells with indicated treatments were seeded into 6-well plates and cultured for 2 weeks. Ten the colonies were fxed in 4% paraformaldehyde for 30 min, followed by staining with 0.1% crystal violet. Colonies were then manually counted.

Scratch-wound healing

Cell migration was determined by performing a scratch-wound healing assay. PDAC cells with indicated treatments were seeded into 24-well plates. Following a 24 h incubation, a wound scratch assay was performed using a pipette tip for each well. Photographs were taken at 0 and 24 h after the scratches were made. The scratch healing rate was calculated by ([1-(area between scratch width at 24 hour/area between scratch width at 0 hour)] × 100%).

Transwell assays

Transwell chambers were used to evaluate migration in the Transwell assays. PDAC cells with indicated treatments were seeded into the upper chamber of a Transwell, and 600 μL of fetal bovine serum-containing medium was placed in the Transwell lower chamber. After 18 h of incubation, the non-migrated cells on the upper side of the chamber membranes were removed. The number of migrated cells in the side of lower chamber was counted from an average of three random visual fields with a microscope.

Polysome fractionation

The Polysome fractionation was performed based on the previously reported protocol. Briefly, the PDAC cells were treated for 5 min with cycloheximide at a final concentration of 100 μg/mL and then lysed with hypotonic buffer. Cytosolic extracts were ultracentrifuged with a 5%–50% sucrose gradient buffer prepared using the Gradient Station (Biocomp). The RNA concentration was calculated with OD260. Fractions were collected with the Gradient Station. RNAs were isolated from sucrose fraction and subjected to qRT-PCR.

RNA isolation and quantitative real-time PCR (qRT–PCR)

Total RNA was isolated with TRIzol (Takara, Japan) and reverse-transcribed using the PrimeScript RT Reagent Kit (Takara, Japan). Then, cDNA was amplified using the TB Green Premix Ex TaqTM kit (RR820A, Takara, Japan) on a Light Cycler 480 Detection System (Roche, Switzerland). β-actin was used as internal control for mRNAs. Primers for PCR were listed in Table S2.

Calculation of PDUI (Percentage of distal PAS usage)

The difference in the usage of proximal PAS and distal PAS in a gene was quantified as the PDUI. To calculate the PDUI, primers for all MZT1 mRNA and for long MZT1 mRNA isoform were designed (Table S2). By qRT-PCR, the CT values of all MZT1 (CT_{all}) and that of long MZT1 isoform (CT_{long}) were obtained. Using β-actin as internal control, the $deltaCT_{all} = CT_{all} - CT_{ACTB}$, and the $deltaCT_{long} = CT_{long} - CT_{ACTB}$. The PDUIs were estimated as follows: $PDUI = [1/(2^{(deltaCTlong - deltaCTall)})] \times 100\%$.

Luciferase reporter assay

3'-UTR reporter vectors were generated by inserting the long 3'-UTR or short 3'UTR sequences of MZT1 into the psiCHECK-2 dual luciferase reporter vector (Promega). Cells were transfected with luciferase reporter and cell extracts were collected 48 hours after transfection. The ratio between firefly and Renilla luciferase was determined using Dual-Luciferase Reporter Assay System (Promega).

RNA immunoprecipitation (RIP) assay

RIP assay was performed by Magna RIP™ RNA-Binding Protein Immunoprecipitation Kit (Millipore, Billerica, MA) according to the manufacturer's protocol. Briefly, cells were lysed using RIP lysis buffer with 0.5 μl protease inhibitor. Magnetic beads were washed twice in RIP wash buffer following incubation with anti-NUDT21 or anti-IgG primary antibody for 3 hours at room temperature. Then the RNA was enriched by washing beads for six times with RIP wash buffer. Purified RNA was subjected to qRT-PCR analysis.

Western blot

Protein was extracted from the cells using RIPA lysis buffer, and the protein concentrations were detected using a bicinchoninic acid Protein Assay Kit (Thermo Scientific). Isolated proteins were separated on SDS-polyacrylamide gels and transferred to a polyvinylidene difluoride membrane (Millipore, Eschborn, Germany). The membranes were then blocked with 5% BSA for 2 h at room temperature, followed by incubation with primary antibodies at 4°C overnight. The following primary antibodies were used: anti-NUDT21 (Abcam), anti-MZT1 (Sigma-Aldrich) and anti-β-actin (Abcam). Then HRP-conjugated secondary antibodies were used. Membranes were washed, and then the proteins were visualized by electrochemiluminescence (Millipore, Germany).

CHX and MG132 assay

Protein translation was blocked by addition of 50 μg/ml cycloheximide (CHX). For MG132 treatment, MG132 (20 μM) was added into cell culture media at 48 h after NUDT21 siRNA transfection and incubated for 6 h at 37°C.

Functional enrichment

RNA-sequencing expression (level 3) profiles and corresponding clinical information for pancreatic cancer were downloaded from the TCGA dataset (https://portal.gdc.com). The enriched KEGG signaling pathways were selected to demonstrate the primary biological actions of

major potential mRNA. The abscissa indicates gene ratio and the enriched pathways were presented in the ordinate. Gene ontology (GO) analysis of potential targets of mRNAs. The biological process (BP), cellular component (CC), and molecular function (MF) of potential targets were clustered based on ClusterProfiler package in R software (version: 3.18.0). Colors represent the significance of differential enrichment, the size of the circles represents the number of genes, the larger the circle, the greater the number of genes. GSEA analysis was performed using WebGestalt algorithms (http://bioinfo.vanderbilt.edu/webgestalt).

QUANTIFICATION AND STATISTICAL ANALYSIS

All statistical analyses were performed using GraphPad Prism 9 and R software (version 4.2.1). Data were presented as the mean $\pm$ SD of independent experiments. The Chi-square test ($\chi 2$ test) was used for categorical data. ANOVA was used for multiple groups and the t test was used to compare continuous variables in two groups. Survival probability was evaluated using Kaplan-Meier curves and long-rank test. Correlations were analyzed by Pearson's correlation test. $p < 0.05$ was set as the threshold for statistical significance unless stated otherwise. *$p<0.05$, **$p<0.01$, ***$p<0.001$.